



Available online at www.sciencedirect.com

ScienceDirect

Comput. Methods Appl. Mech. Engrg. 345 (2019) 52-74

Computer methods in applied mechanics and engineering

www.elsevier.com/locate/cma

An adaptive isogeometric analysis collocation method with a recovery-based error estimator

Yue Jia^{a,b}, Cosmin Anitescu^{c,*}, Yongjie Jessica Zhang^b, Timon Rabczuk^d

^a School of Mechanics, Civil Engineering and Architecture, Northwestern Polytechnical University, China

^b Department of Mechanical Engineering, Carnegie Mellon University, USA

^c Institute of Structural Mechanics, Bauhaus-Universität Weimar, Germany

^d Department of Computer Engineering, College of Computer and Information Sciences, King Saud University, Riyadh, Saudi Arabia

Received 16 July 2018; received in revised form 25 October 2018; accepted 25 October 2018

Available online 3 November 2018

Highlights

- Isogeometric collocation at Gauss points leads to an optimally convergent scheme.
- A hybrid Galerkin-collocation method is used for the patch and Neumann boundaries.
- Adaptive refinement with PHT splines is driven by a recovery-based error estimator.

Abstract

In this paper, we propose an enhanced isogeometric analysis (IGA) collocation method. It is well known that the location of the collocation points plays an important role in the accuracy and stability of IGA collocation methods. This is particularly true for non-uniform meshes and domains generated from multi-patch geometries. We present an enhanced collocation method based on Gauss points, which has improved accuracy as compared to using C^1 splines and a recovery-based error estimator that can be derived by sampling the solution at particular points in the domain. Adaptivity is implemented using a hierarchical spline basis, which satisfies the C^1 continuity requirement. The proposed approach has been tested by several benchmark problems, including multipatch domains and geometries with re-entrant corners.

© 2018 Elsevier B.V. All rights reserved.

Keywords: IGA collocation method; Gaussian-collocation points; PHT-spline; Linear elasticity; Error estimation

1. Introduction

Isogeometric analysis (IGA) is a numerical method introduced by Hughes et al. [1,2] in 2005 aiming to bridge the computer aided design (CAD) and the finite element analysis (FEA). It applies the same spline basis for the seemetry design and the numerical analysis without re-meshing the CAD model. IGA has been shown to possess



The Trial Version

@syr.edu (C. Anitescu).

.2018.10.039

0045-7825/© 2018 Elsevier B.V. All rights reserved.

several advantages for solving engineering problems. Since the classical basis of IGA are Non-uniform rational B-splines (NURBS), it can provide higher order continuity required, such as for Kirchhoff–Love shell models [3,4]. In recent work, commercial software packages such as ABAQUS [5], FEAP [6] and LS-DYNA [7] have been extended to use IGA solvers for advanced industrial computing applications.

The traditional IGA is based on NURBS, for which adaptive refinement cannot be localized due to the tensor-product structure of the basis. In 2003, Sederberg [8] proposed T-splines which allow T-junctions in the refined mesh. The T-splines are useful for constructing un-structured meshes for geometrical design. In recent years, analysis suitable T-splines have been developed and used in IGA solvers [9,10]. Moreover, IGA has also been successfully used with several other spline spaces which have local adaptivity properties, such as the PHT-splines [11], THB-splines [12], LR-B splines [13] and truncated T-splines [14]. Many of these spline spaces have been subject to theoretical research for CAD-oriented applications as well.

Most of the commonly used partial differential equation (PDE) solvers are based on the so-called weak (or variational) form. The Gauss quadrature is commonly used in IGA integral calculations. However, as the order of the polynomial degree increases, more quadrature points are needed to accurately evaluate the resulting integrals, which affects the computational efficiency significantly [15]. For the IGA method in particular, several reduced-quadrature methods [16] and other customized quadrature rules [17–19] have been developed over the years. The IGA collocation is another approach, which eliminates the integration and discretizes the strong form of the PDEs directly. The IGA collocation has been developed since 2010 [20–24] and, to a large extent, it combines the advantages of the accuracy and smoothness from the IGA method with the computational efficiency of the collocation method. In IGA collocation, Greville abscissae [25] are usually chosen as the collocation points, which has some advantages, such as the one-to-one correspondence between the collocation points and basis functions. However, finding the optimal collocation points is still an open and challenging research problem. For example, in order to improve the convergence rates, the IGA collocation based on superconvergent points has been introduced in [26] and further studied in [27,28]. But collocating at the superconvergent points can result in an over-determined system which has to be solved in a least square sense. Furthermore, imposing boundary conditions for IGA collocation is another concern, as properly imposing boundary collocation points and defining the boundary discretization equations influence the accuracy and stability of the results. In [29], it has been shown that oscillations in the numerical results may arise from the boundary value calculations and more constrains need to be applied on the boundary system portion. To reduce the effects from the collocation boundary points, a hybrid Galerkin-collocation technique was proposed [30]. It replaces the collocation boundary entries by the corresponding Galerkin ones. This method was described to some extent in the research of the isogeometric collocation for phase-field fracture models [30]. But to the best of our knowledge, the method was not studied in great detail.

The adaptivity must be driven by a certain method, which is commonly defined by error estimators or error indicators. While error estimators attempt to quantify the error in the approximation over each element, error indicators can be used to determine areas with large errors. Since 1970s, the error estimators have been studied for the FEM discretizations [31,32]. Currently, there are two main types of error estimators: the residual based and the recovery based. Our research is mainly focused on the latter case. The main idea is to compute a recovered solution which is obtained by sampling the computed solution at chosen points. The sampling is performed at points (such as superconvergent points) which are known to have higher accuracy. By fitting these values with a higher order polynomial functions, it is possible to obtain a recovered solution which will be better (closer to the unknown exact solution) than the computed solution. Then the estimated error can be used as an approximation of the actual error, which is the difference between the exact solution and the computed solution. From a theoretical point of view, the superconvergence only holds for the quasi-uniform discretizations with smooth solutions. However, in practice, the error estimator can be used on non-uniform meshes with singular solutions as an error indicator [33]. For most engineering problems, it is impossible to find analytical solutions, but we can still calculate the recovered solution and carry out error estimation. The early FEM related research on patch-recovery has been developed in [34,35].

error estimation methods for IGA solvers. For example in [36], a multi-level estimation by applying bubble functions in T-splines analysis. In [37], a residual based error estimation ne based IGA. However, compared to FEM, the application of the error estimation in IGA is

The Trial Version Pedia bose an adaptive IGA collocation method based on the PHT-spline basis. Considering the C^1 continuity of PHT-spline-elements, we choose Gauss points as our collocation points, which will lead to an optimal scheme as shown in [38]. A hybrid collocation approach is presented, combining the interior collocation elements

pdfelement

with the outer Galerkin boundary. Elimination and relocation techniques for the Gaussian collocation points around the T-junction regions can guarantee a fully determined system and compatible numerical results. The adaptivity is driven by a particular recovery error estimator, which is based on the computed solution. In our research, we have applied the proposed method to 2D and 3D elasticity problems containing multiple patches and the re-entrant corners. We also obtain the same convergence rates for both uniform and adaptive solving procedures as compared with Galerkin methods.

The paper is organized as follows: in Section 2, we briefly review the PHT-spline basis, and moreover, we introduce the hybrid Gaussian collocation method. The recovery error estimator is illustrated in Section 3. The numerical experiments to validate the method are presented in Section 4. The paper ends with a brief summary in Section 5.

2. IGA collocation methods

2.1. Overview of point collocation for spline approximation spaces

In a general setting, we consider a boundary value problem of the form:

$$\mathcal{L}(\mathbf{u}(\mathbf{x})) = \mathbf{f}(\mathbf{x}) \text{ for } \mathbf{x} \in \Omega,$$

$$\mathcal{L}(\mathbf{u}(\mathbf{x})) = \mathbf{g}(\mathbf{x}) \text{ for } \mathbf{x} \in \partial\Omega,$$
(1)

where \mathscr{L} and \mathscr{G} are differential operators, $\Omega \subset \mathbb{R}^d$ is the computational (physical) domain with boundary $\partial \Omega$ and $\mathbf{f}: \Omega \to \mathbb{R}^n, \mathbf{g}: \partial \Omega \to \mathbb{R}^n$ are given functions.

As usual in IGA, we consider a parameter space $\Omega_{par} := [0, 1]^d$ which is mapped to the physical domain Ω by a mapping $\mathbf{F} : \Omega_{par} \to \Omega$. The mapping can be described by a set of spline (e.g. B-Spline or NURBS) basis functions and the associated control points, i.e.

$$\mathbf{F}(\boldsymbol{\xi}) := \sum_{i=1}^{N} \mathbf{C}_{i} \phi_{i}(\boldsymbol{\xi}) \text{ for } \boldsymbol{\xi} \in \Omega_{\text{par}},$$
(2)

where C_i are the d-dimensional control points, and ϕ_i are the spline basis functions.

The main idea of the collocation method is to select a set of points $\mathbf{x}_i^* \in \Omega \cup \partial \Omega$ for which the differential equation (1) holds with the approximate solution \mathbf{u}_h^C , i.e.

$$\mathbf{u}_{h}^{C}(\mathbf{x}) = \sum_{i=1}^{n} \mathbf{D}_{i} \phi_{i} \circ \mathbf{F}^{-1}(\mathbf{x}), \tag{3}$$

where \mathbf{D}_i are *n*-dimensional solution coefficients chosen to satisfy:

$$\mathcal{L}(\mathbf{u}(\mathbf{x}_i)) = \mathbf{f}(\mathbf{x}_i) \text{ for } \mathbf{x}_i \in \Omega,$$

$$\mathcal{L}(\mathbf{u}(\mathbf{x}_i)) = \mathbf{g}(\mathbf{x}_i) \text{ for } \mathbf{x}_i \in \partial\Omega.$$
(4)

Different choices of the points \mathbf{x}_i and basis functions ϕ_i give rise to different collocation schemes. Note that for a mth order differential operator \mathcal{L} , it is desirable for the approximation space spanned by $\phi_i \circ \mathbf{F}^{-1}$ to have C^{m-1} continuity. While spline basis functions of quadratic and higher degree can easily fulfill this requirement, special treatment is needed in the case where the continuity is reduced, such as in the case of repeated knots or at the patch interfaces. We will detail some methods of dealing with this in Section 2.3.

In the following, we give a brief overview of the choices of collocation points that can be considered.

2.1.1. Greville abscissae collocation

The traditional collocation points are chosen to be Greville abscissae [20]. For a given knot vector $\Xi = \{\xi_1, \xi_2, \dots, \xi_{n+p+1}\}$, the associated Greville abscissae points $\bar{\xi}_i$ ($i = 1, \dots, n$) are defined by

$$\frac{+\cdots+\xi_{i+p}}{p}.$$
 (5)

pdfelement

The Trial Version $+\cdots + \xi_{i+p}$ per Greville abstraction total basis fur

re Greville abscissae points are computed directly from knot vector and the number of points total basis functions in the approximation space, which results in a fully determined linear is been shown that the collocation method based on the Greville abscissae is less accurate;

in addition, it exhibits sub-optimal convergence in energy (H^1) norm for odd polynomial degrees. Moreover, local adaptive refinement requires the use of T-Splines [39] or a weighting procedure [23].

2.1.2. Collocation at superconvergent points

A different strategy for selecting collocation at superconvergent points was developed in [26] based on numerical results, which provides optimal convergence rates in the first derivative (energy) norms for all polynomial degrees. The idea is to use the superconvergent points of the second derivative of the Galerkin solution as the collocation points. These points are calculated based on the mesh discretization only, whereas they can be computed on a reference element and the obtained coordinates can then be mapped onto any quasi-uniform mesh.

2.1.3. Gaussian collocation

It has been observed that when cubic spline spaces are considered, the superconvergent points for the second derivative are the Gauss points. In [38], it has been proven in 1D that collocating at Gauss points leads to optimal convergence rates for B-splines of any degree but with reduced (C^1) continuity. Moreover, even higher convergence rates can be obtained at particular points such as at the knots (element vertices). In this paper, we investigate the use of Gaussian collocation with C^1 cubic splines where PHT-splines are adopted to obtain hierarchical and local refinement. As shown in the next section, the PHT-splines are constructed with C^1 continuity, therefore they are a particularly well suited basis for Gaussian collocation. The higher approximation rate can be used to construct a recovery-based error estimator, as shown in Section 3.

2.2. Cubic splines over hierarchical T-meshes

PHT-splines are defined on hierarchical T-meshes, which have different refinement levels. Elements at a finer refinement level are generated by a cross insertion procedure. At each cross insertion, a refined element is subdivided into 4 elements in 2D and 8 elements in 3D. Fig. 1 illustrates the process of generating a hierarchical T-mesh with three levels. The refined meshes contain three types of vertices, which are either boundary vertices, crossing vertices or T-junctions. The first two are denoted as *basis vertices*, since they are associated with particular basis functions in the mesh. In Fig. 1, we show these three types of vertices generated by the cross insertion. For cubic polynomials, each basis vertex is associated with 4 basis functions for 2D problems and with 16 basis functions for 3D problems. There are no basis functions associated with the T-junctions.

The PHT-splines are constructed level by level. In the following, we will briefly review the construction of the basis functions. In the 2D case, each cubic basis function ϕ on an element E can be represented as a linear combination of 16 Bernstein basis functions. Their coefficients are called Bézier ordinates. This process is also called Bézier extraction [40]. We define a linear mapping \mathbf{F}_R from a reference element $[-1, 1] \times [-1, 1]$ to the current element E_K in the parameter space $[0, 1] \times [0, 1]$. Then the basis function ϕ in the parameter space is represented by

$$\phi(\xi,\eta) = \sum_{i=1}^{4} \sum_{j=1}^{4} C_{ij} B_{ij} \circ \mathbf{F}^{-1}(\xi,\eta), \tag{6}$$

where $B_{ij}(\hat{\xi}, \hat{\eta}) = B_i(\hat{\xi})B_j(\hat{\eta})$ is a tensor product of Bernstein polynomials defined on the reference interval [-1, 1]. We have

$$B_i(\xi) = \frac{1}{2^p} \binom{p}{i-1} (1-\xi)^{p-i+1} (1+\xi)^{i-1}, \qquad i = 1, 2, 3, 4$$
 (7)

where C_{ij} are the Bézier coefficients and they can be calculated through the De Casteljau's algorithm [25]. For the details of computing the Bézier coefficients we refer to [40].

To keep the linear independence of the basis and better sparsity in the resulting matrix solving system, a truncation procedure is employed after the cross insertion. A detailed discussion is given in [33]. Fig. 2(a) shows the node indices in a cubic mesh. After the cross insertion, there are three new basis vertices, including one crossing vertex and two boundary vertices, which yield new basis functions as shown in Fig. 2(b). The two T-junctions do not create new basis

pdfelement

The Trial Version

k+1 representing the current refined mesh. Thus, the previous step mesh is at level k. In independence of the new basis at level k+1, some basis functions from the level k need to le, Fig. 3 shows a cubic basis function before (Fig. 3(a)) and after (Fig. 3(b)) the truncation ction is represented by 16 Bézier ordinates in each element. The initial Bézier coordinates are refinement, we apply the De Casteljau's algorithm to define the Bézier coordinates associated

to the four new elements as shown in Fig. 3(d). Then we zero out all the Bézier entries surrounding the basis vertex, and finally obtain the basis in Fig. 3(e).

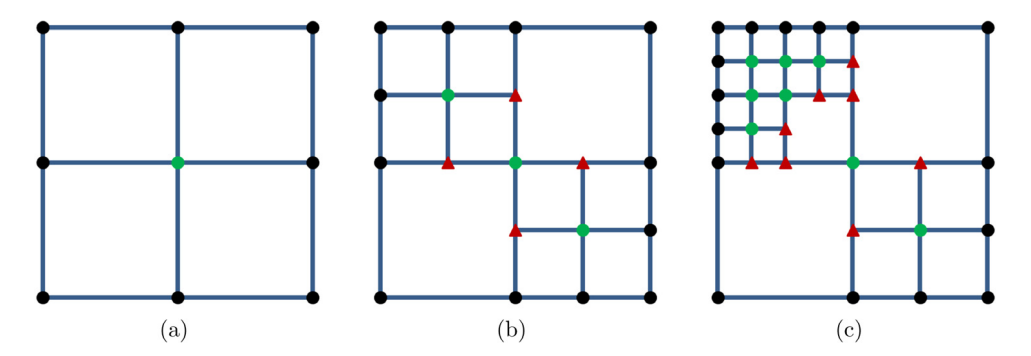


Fig. 1. Illustration of the boundary vertices, crossing vertices and T-junctions: (a) the initial mesh; and (b)–(c) after cross insertion refinements. The black dots denote the boundary vertices, the green dots represent the crossing vertices and the red triangles are T-junctions. (For interpretation of the references to color in this figure legend, the reader is referred to the web version of this article.)

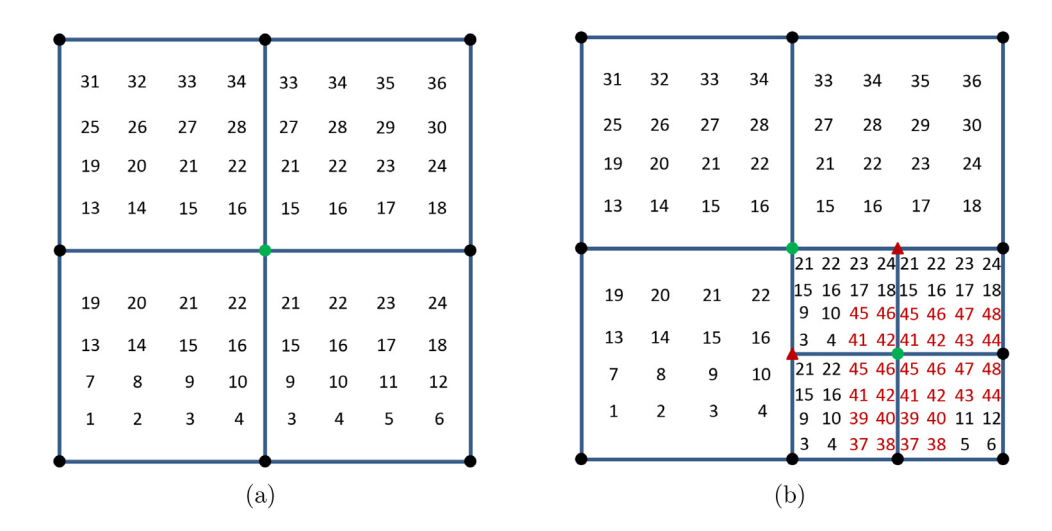


Fig. 2. Global basis indices on each element for p = 3.

2.3. Hybrid IGA Gaussian collocation method

In the following, we give an overview of the hybrid Gaussian collocation method, which can be used to improve the approximation at the Neumann boundary and in regions of the domain for which the regularity requirements for collocation are not satisfied. These include the patch boundaries in multi-patch geometries for which normally only C^0 continuity is achieved, as well as points of singularity in the exact solution such as re-entrant corners. The main observation is that two types of test functions can be considered: the Dirac-delta functions $\delta(x-x^*)$, where x^* is a collocation point for the collocation part, and the standard spline functions for the Galerkin part. The Dirac-delta functions have the following property:

$$f(x)\delta(x-x^*) = f(x^*)$$
which is continuous at $x^* \in \Omega$.

The Trial Version that $a(\mathbf{u}, \mathbf{v}) = f(\mathbf{v})$ for all $\mathbf{v} \in W$, (9)

where V and W are suitable spaces containing the test and trial functions respectively and f is the right-hand side functional which incorporates the body forces and Neumann boundary conditions. In the standard Galerkin method,

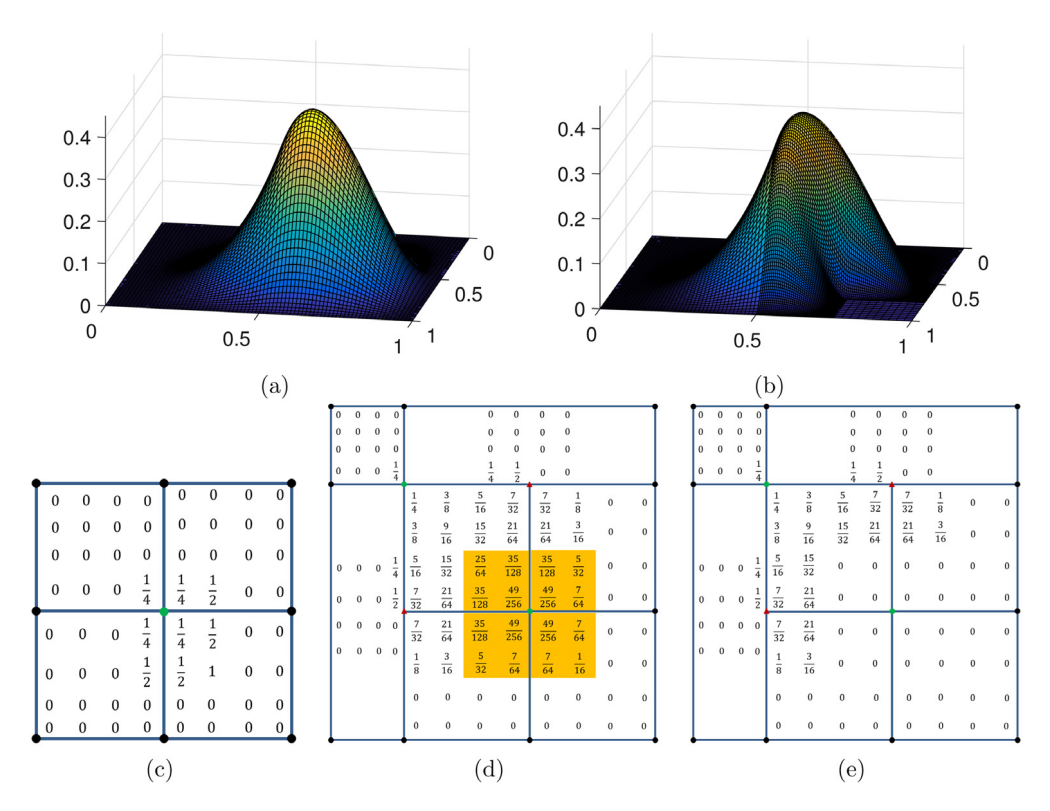


Fig. 3. Modification of a cubic (p = 3) basis function: (a) before truncation; (b) after truncation; (c) initial Bézier ordinates on the unrefined element; (d) subdivision of one element into four subcells. The squared shaded ordinates correspond to the new basis vertex; and (e) the Bézier ordinates around the new basis vertex are set to zero.

the test and trial spaces are identical, containing spline approximation functions, while in the pure collocation method the W space consists of Dirac delta functions. In hybrid Gaussian collocation, we consider a test space W which consists of both types of functions. Then the linear system is assembled in the standard way:

$$K_{ii} = a(\phi_i, \psi_i), \tag{10}$$

where ϕ_i are PHT spline basis functions and ψ_j are either the Dirac-deltas or the PHT splines. Each row of the resulting system matrix corresponds to a test function and each column to a trial function. The bilinear form is an integral over the whole domain, however the entries are evaluated in an element-wise assembly subroutine only on the elements where the Galerkin basis functions have support.

2.4. Obtaining a fully determined linear system

Fig. 4 illustrates the solving procedure and the construction of the linear system in two dimensions. The problem domain is discretized into two patches. There are 66 basis functions in total. The green dots represent 32 collocation points. The red numbers identify the 30 boundary basis functions. The numbers enclosed in yellow squares stand for

ary basis functions. Thus we have found 66 constrains for the problem, which result in a fully m. Note that for the multi-patch modeling, the rows from the Galerkin system corresponding lary basis have to be added to the collocation system to ensure the number of the rows is the olumns. To have a fully determined system, the total number of collocation points needs to be r of basis functions. For the uniform refinement strategy, since there are 4 collocation points

per element, this condition is automatically satisfied. However for adaptive refinement, keeping 4 collocation points in the elements around T-junctions will result in more collocation points than basis functions. This is because each

13	14	30	32	30	32	15	16	16	46	60 62	60 62	47	48
9	10	29	31	29	31	11	12	12	43	59 61	59 61	44	45
18	20	34	36	34	36	22	24	24	50	64_66	64_66	52	54
17	19	33	35	33	35	21	23	23	49	63 65	63 65	51	53
18	20	34	36	34	36	22	24	24	50	64 66	64 66	52	54
17	19	33	35	33	35	21	23	23	49	63 65	63 65	51	53
5	6	26	28	26	28	7	8	8	40	56 58	56 58	41	42
1	2	25	27	25	27	3	4	4	37	55 57	55 57	38	39

Fig. 4. Collocation points and basis functions distribution on two patches with cubic polynomial degree. (For interpretation of the references to color in this figure legend, the reader is referred to the web version of this article.)

basis vertex is associated with 4 collocation points. Since T-junctions are not basis vertices, they do not generate new basis functions. Thus, we do not need to consider any collocation points associated with T-junctions.

Another issue is the position of the collocation points which needs to be adjusted according to the distance from the nearest basis vertex. In the case of uniform mesh, there will be one Gauss point in each of the four elements adjacent to the basis vertex, resulting in a one-to-one correspondence between the basis functions and the collocation points. The same principle is used in the case of adaptive meshes with T-junctions. For example in Fig. 5, we show a mesh where some elements have 2 or 3 collocation points (red dots). Fig. 5(e) shows how the relocation technique works, where the green dot is a given basis vertex. Its support is marked by four edges (the left-edge in orange, the right-edge in red, the down-edge in brown and the up-edge in yellow). There are four collocation points associated to this basis vertex. The collocation point-1 is defined by the left-edge and the up-edge. The collocation point-2 is defined by the right-edge and the up-edge. The point-3 is defined by the left-edge and the down-edge. The point-4 is defined by the right-edge and the down-edge. In this example, since the left-edge is equal to the right-edge, the four collocation points have equal distances to the basis vertex in the horizontal direction. Since the up-edge is shorter than the down-edge, the point-1 and point-2 are closer to the basis vertex than the collocation point-3 and point-4 in the vertical direction. This relocation rule is used for all the collocation points in the mesh and is implemented in a similar way for three-dimensional domains.

3. Recovery-based error estimation

The recovery estimator is obtained from a recovered solution which involves sampling the computed solution at several chosen points. To ensure a reliable estimator, the sample points should be chosen at carefully selected points where the solution is known to be accurate. In the finite element method, a common choice is to use Gauss quadrature points, which have been shown to be superconvergent for the approximation spaces of Lagrange polynomials [41,42]. However, for the case of spline-based approximation spaces, superconvergence is obtained at different points which can be calculated as the roots of a polynomial function [26,33]. For the Galerkin's method, this function can be written in terms of the difference between a monomial of degree p+1 and its interpolant in the spline approximation space. In the following, we show how the superconvergent points can be computed for collocation methods, in particular for collocation at Gauss points.

As in the Galerkin case, for the 1-dimensional setting, we consider $Q(x) = x^{p+1}$ to be a monomial of degree p+1. We let S^h be the space of C^1 splines of degree p with knots at x_0, \ldots, x_n . We then define $I^h[Q](x) \in S^h$ to be the interpolant of Q(x) and its derivative at the mesh vertices (knots), i.e.

$$\frac{d^{\alpha}I^{h}[O]}{dx^{\alpha}}(x_{i}) = \frac{d^{\alpha}Q}{dx^{\alpha}}(x_{i}), \quad \alpha = 0, 1, \quad \text{and} \quad i = 0, \dots, n.$$
(11)

here are exactly two shape functions with non-zero value and derivative at each mesh vertex. ant can be determined by solving a 2×2 linear system corresponding to each vertex, and we

pdfelement

 $I^{h}[Q](x) = \sum_{k=1}^{\infty} c_k \phi_k(x), \tag{12}$

The Trial Version

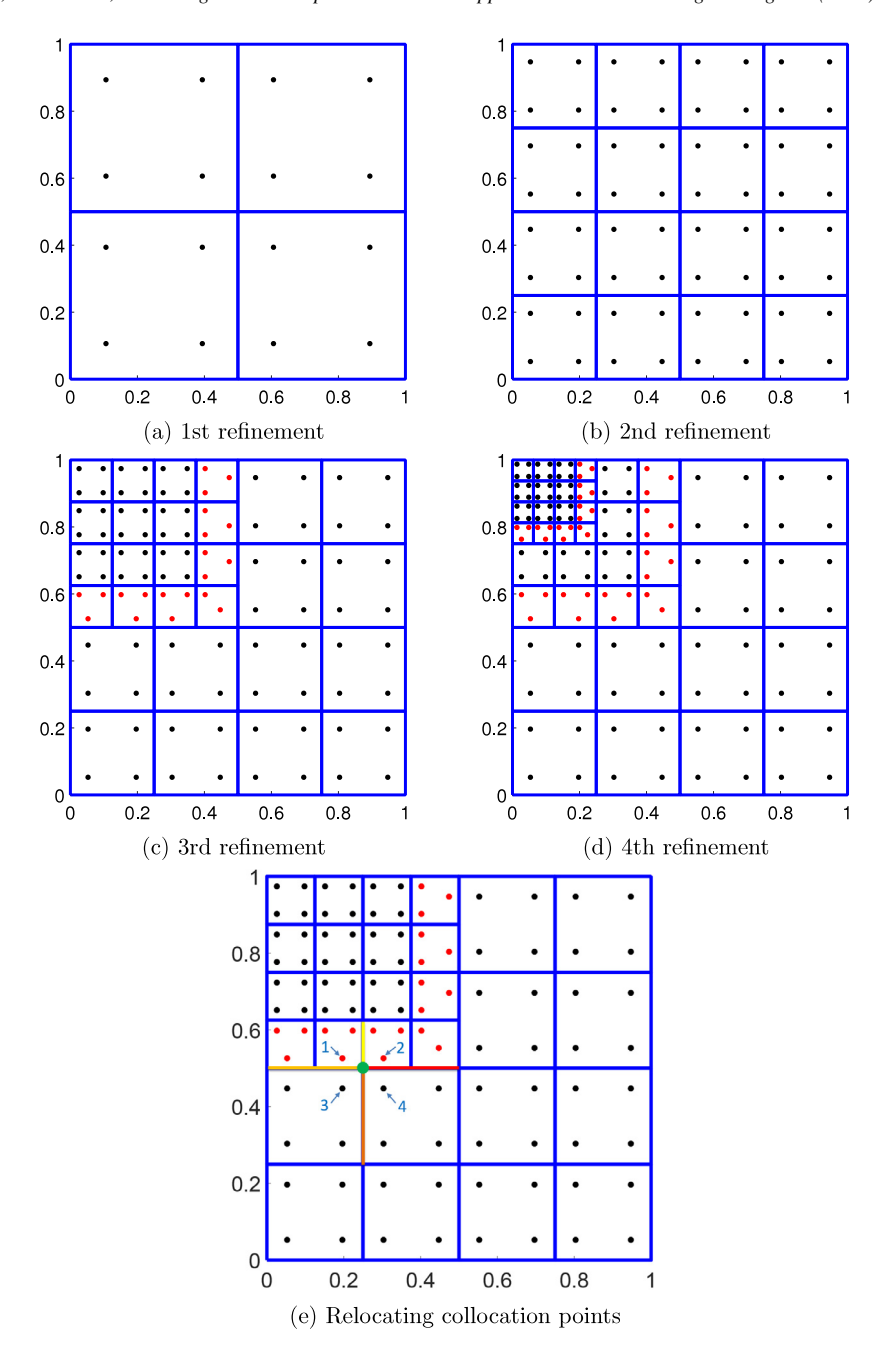


Fig. 5. The refined meshes and distribution of collocation points. (For interpretation of the references to color in this figure legend, the reader is referred to the web version of this article.)

pdfelement
The Trial Version

spline basis functions and c_k are the interpolation coefficients. For the interior vertices, an be determined by solving a linear system of the form

Furthermore, the elements of the left-hand side of the matrix in (13) depend only on the knot distances between x_i and its immediate neighbors [11].

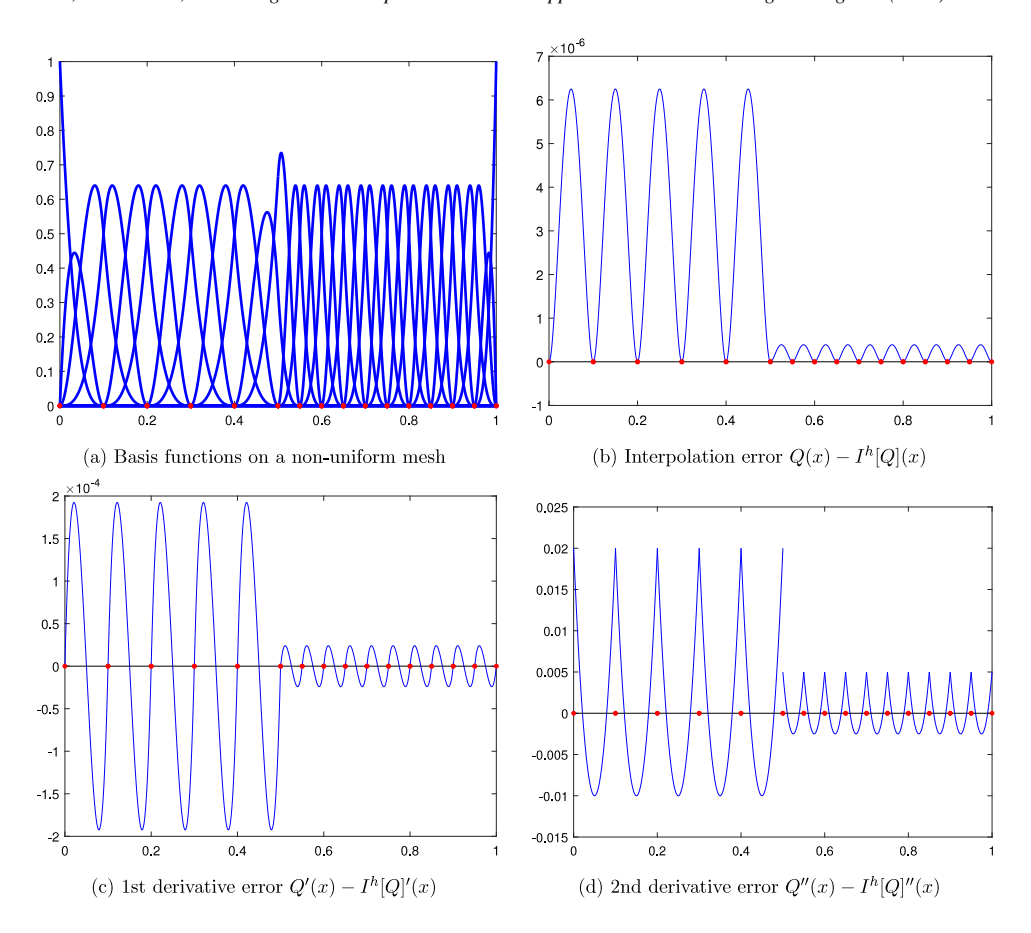


Fig. 6. Interpolation error for the function $Q(x) = x^4$ with cubic C^1 splines.

We now let x_k^* for $k=1,\ldots,2n-2$, denote the Gaussian collocation points defined by the 2-point Gauss rule on each of the elements (x_i,x_{i+1}) , and obtain $x_i^{\text{mid}}=(x_i+x_{i+1})/2$ for $i=1,\ldots,n-1$. It is easy to check that

$$I^{h}[Q]'(x_i^{\text{mid}}) = Q'(x_i^{\text{mid}}) \tag{14}$$

and

$$I^{h}[Q]''(x_{k}^{*}) = Q''(x_{k}^{*}). \tag{15}$$

Eq. (15) immediately implies that $I^h[Q] = Q_h^C$, where Q_h^C is the Gaussian collocation solution to the boundary value problem:

$$-Q''(x) = 12x^2, \text{ for } x \in (x_0, x_n)$$

$$Q(x_0) = x_0^4, \quad Q(x_n) = x_n^4,$$
(16)

which has the exact solution $Q(x) = x^4$. Then from (14) and by the arguments presented in [38], the collocation pregent in the first derivative at the element vertices as well as at the element midpoints. In sis functions and approximation error on a non-uniform mesh where the elements size of the l by a factor of 2.

The Trial Version is superconvergent points for the first derivative are the same as in the case of the Galerkin method ubic splines, as shown in [33]. Then we can define the recovery patches consisting of two neighboring elements, which result in 5 superconvergent points that can be fitted by 5 cubic splines with C^2 interelement continuity. Since the derivatives of the computed solution (which are piecewise quadratics) are fitted by cubic

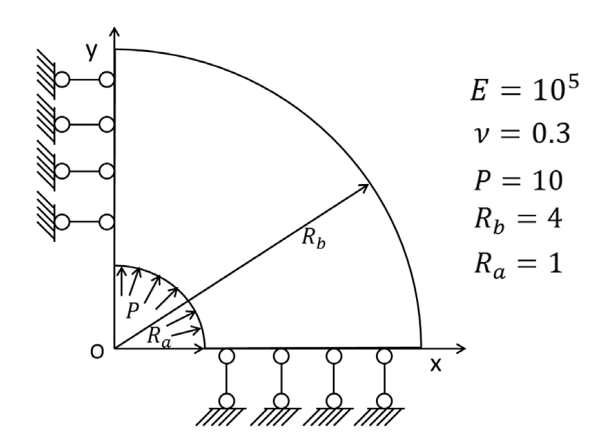


Fig. 7. Problem description for the annulus example.

functions, the resulting recovered gradient solution is of higher order. The recovery procedure can be easily extended to higher-dimensional domains by taking advantage of the local tensor-product structure inherent to the hierarchical meshes.

After computing the estimated error, it is important to use an appropriate marking scheme to select the to-berefined elements. Our approach is based on the Döerfler method [43], which marks the elements contributing up to ρ percentage of the total estimated error. In [33], it was determined that the Döerfler marking gives better results (at the cost of possibly more refinement steps), than marking all the elements exceeding a prescribed threshold. In general, the parameter $\rho \in (0, 1]$. Note that $\rho = 1$ results in uniform refinement, while $\rho \ll 1$ results in smaller refinement steps. There is always a trade-off between the number of refinement steps and the "optimality" of the refinement. In practice, we choose $\rho = 0.75$ for problems with smooth solutions, and $\rho = 0.5$ for problems containing singularities.

The theoretical justification for higher dimensions and for geometry mappings to the physical space which are not fully regular has not been fully developed. Nevertheless, in Section 4 we provide evidence that the recovery-based error estimator is sufficiently robust to drive the adaptive algorithm.

4. Numerical examples

In this section, we present five examples, ranging from 2D to 3D elasticity problems for which an analytical solution is available. We show that optimal convergence rates can be achieved by the proposed Gaussian collocation method, compared with the traditional Greville collocation and the Galerkin approaches.

4.1. Pressurized cylinder modeled by a quarter-annulus domain

We first consider a benchmark problem of a quarter-annulus subjected to a pressure at the inner circular edge. The model is described in Fig. 7. A plane stress state is assumed. The exact solution for the stress components [44] in polar coordinates is

$$\sigma_{rr} = \frac{R_i^2 P}{R_a^2 - R_b^2} \left(1 - \frac{R_a^2}{r^2} \right),\tag{17}$$

$$\tau_{i,i} = \frac{R_i^2 P}{R_i^2 - R_i^2} \left(1 + \frac{R_a^2}{r^2} \right),\tag{18}$$

pdfelement (19)

The Trial Version stand for the inner and outer radius, respectively. P is the pressure exerting along the inner circular radius the adaptivity is given by the recovery error estimator. The collocation points around the T-junctions need to be eliminated and relocated as shown in Fig. 8. Since the number of refined elements is driven by the parameter ρ , it may happen that not all the elements with the same estimated error are marked for refinement. The refining procedure stops

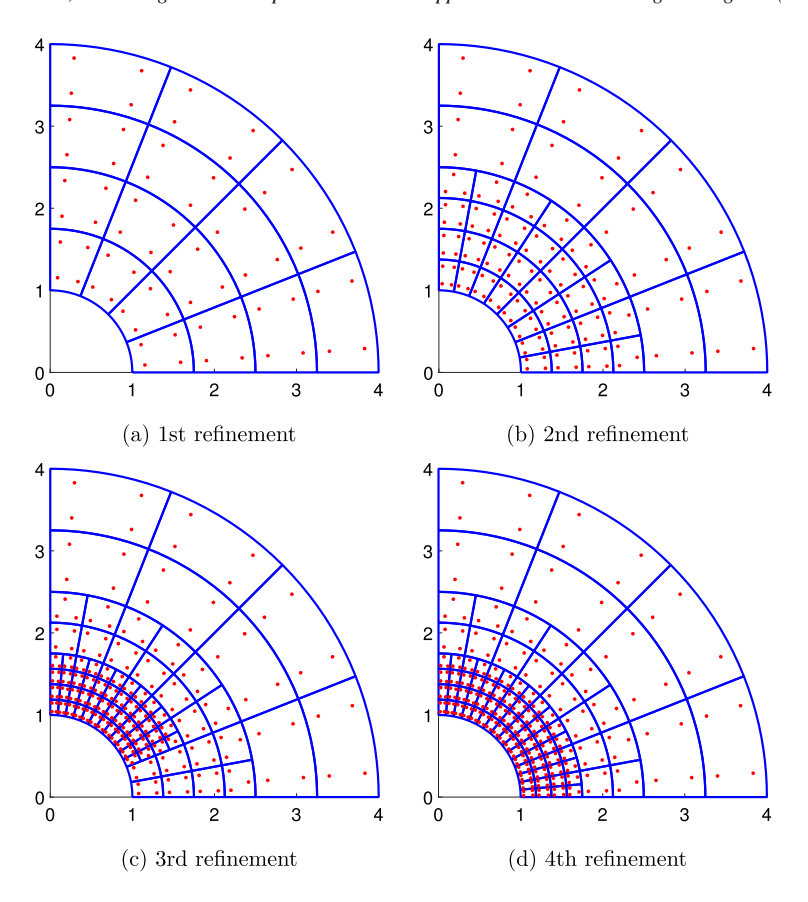
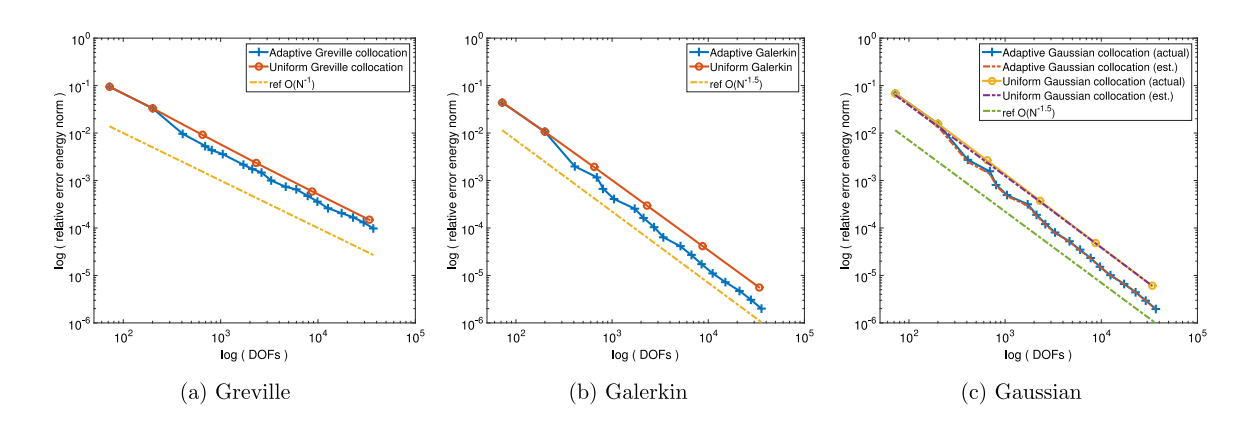


Fig. 8. The refined meshes and the distribution of collocation points in the annulus example.



ror (exact and estimated) in energy norm, using adaptive and uniform refinements for the annulus example.

the Trial Version he estimated error of the marked elements reaches the target percentage of the total estimated 8(c). With the point elimination and relocation techniques, the Gaussian collocation yields the optimal convergence rates, with similar performance to the IGA Galerkin approximation as shown in Fig. 9, whereas the Greville collocation converges only at a sub-optimal rate.

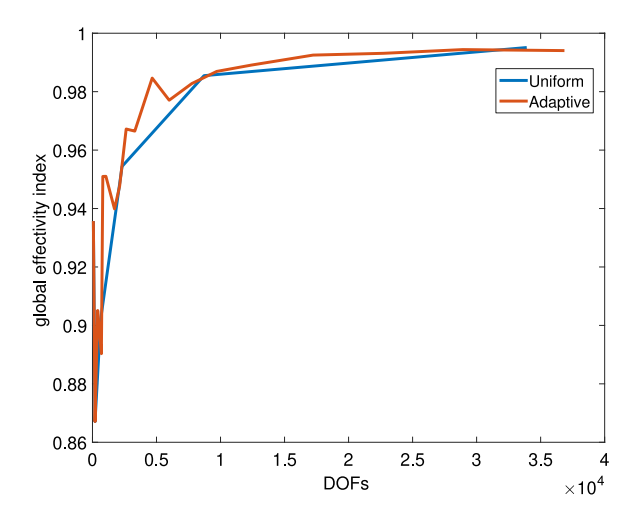


Fig. 10. The global effectivity index plot for the annulus model.

The error estimators are evaluated both locally and globally. This evaluation is based on the effectivity of the error in the energy norm. The global effectivity index is defined as

$$\theta = \frac{\|\mathbf{e}_{es}\|}{\|\mathbf{e}\|},\tag{20}$$

where \mathbf{e}_{es} represents the estimated error and \mathbf{e} stands for the actual error. In our research, we choose the superconvergent points and then fit these values with higher order spline functions. The assumption is that the recovered solution will be closer to the unknown exact solution. If this is true, then θ should approach to 1 asymptotically. In theory, superconvergence only holds for uniform meshes and smooth solutions, but in practice, it holds even on non-uniform meshes and singular solutions, where areas with larger errors are refined first. Fig. 10 is the global index plot of the annulus model solved by the proposed Gaussian collocation method. The global effectivity indices for both uniform and adaptive refinement are approaching 1 with mesh refinement. The quality of the estimator can also be studied at a local level by computing the local effectivity index named D, which is based on the robustness index described in [45,46]. D represents the variation of the effectivity index in each element with the following expression

$$D = \begin{cases} \theta^{e} - 1 & \text{if } \theta^{e} \ge 1 \\ 1 - \frac{1}{\theta^{e}} & \text{otherwise} \end{cases} \text{ with } \theta^{e} = \frac{\|\mathbf{e}_{es}^{e}\|}{\|\mathbf{e}^{e}\|},$$
 (21)

where *e* represents the element level. A good error estimator yields values of *D* close to zero. For more detailed discussion about the local effectivity index, we refer to [46]. In Fig. 11, we plot the local effectivity index for the annulus model. As we can observe, more negative local effectivity index values appear around the blending elements between two levels. There are two possible reasons for this phenomenon. One is the truncation of the PHT basis can result in the decay phenomenon, as discussed in [47]. The other reason is the PHT basis is not a tensor product function, and the support of several basis functions around T-junctions is cut by the truncation technique [11,47]. However, in practice, the recovery error estimator is still a good indicator for local refinement, with improved approximation and optimal convergence rates as shown in the following numerical examples.

pdfelement

The Trial Version

ir note

is a standard benchmark problem of an infinite plate with a hole in plane stress shown in blem numerically, we only consider a finite domain. The exact solution [48] is given in terms

$$\sigma_{rr}(r,\theta) = \frac{T_x}{2} \left(1 - \frac{R^2}{r^2} \right) + \frac{T_x}{2} \left(1 + 3\frac{R^4}{r^4} - 4\frac{R^2}{r^2} \right) \cos 2\theta, \tag{22}$$

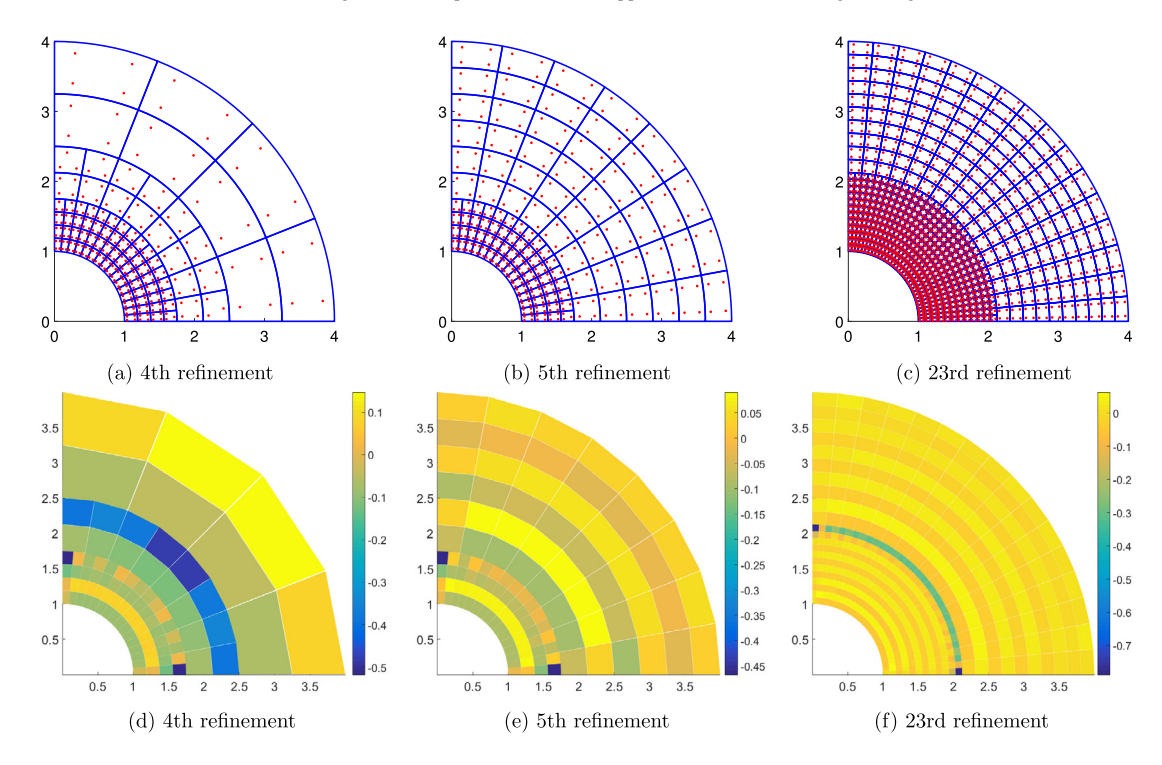


Fig. 11. Local effectivity index D (ideal value D = 0). (a), (b) and (c) are the structured mesh. (d), (e) and (f) are the corresponding local effectivity index plots.

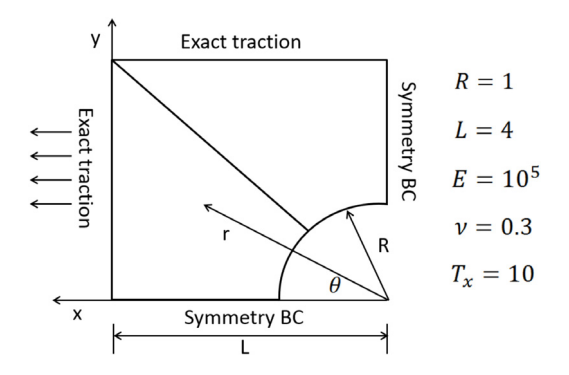


Fig. 12. Problem description for the plate with a circular hole example.

$$\sigma_{\theta\theta}(r,\theta) = \frac{T_x}{2} \left(1 + \frac{R^2}{r^2} \right) - \frac{T_x}{2} \left(1 + 3\frac{R^4}{r^4} \right) \cos 2\theta, \tag{23}$$

$$\sigma_{r\theta}(r,\theta) = -\frac{T_x}{2} \left(1 + 2\frac{R^2}{r^2} - 3\frac{R^4}{r^4} \right) \sin 2\theta, \tag{24}$$

adius and angle with respect to the origin which is located in the center of the hole. The stresses nates system are given by

The Trial Version

pdfelement

$$\begin{pmatrix} \sigma_{yy}(x, y) \\ \sigma_{xy}(x, y) \end{pmatrix} = A^{-1} \begin{pmatrix} \sigma_{rr}(r, \theta) \\ \sigma_{\theta\theta}(r, \theta) \\ \sigma_{r\theta}(r, \theta) \end{pmatrix},$$
(25)

where the transformation matrix A is

$$A = \begin{pmatrix} \cos^{2}(\theta) & \sin^{2}(\theta) & 2\sin(\theta)\cos(\theta) \\ \sin^{2}(\theta) & \cos^{2}(\theta) & -2\sin(\theta)\cos(\theta) \\ -\sin(\theta)\cos(\theta) & \sin(\theta)\cos(\theta) & \cos^{2}(\theta) - \sin^{2}(\theta) \end{pmatrix}.$$
 (26)

The discretization on the coarse mesh has two PHT patches, which contain a C^0 line at the patch boundary. The refined elements and the relative errors obtained in x-direction stress (σ_{xx}) are shown in Fig. 13. It can be observed that the region with a large error contribution is captured by the adaptivity and the error is decreasing. We also compare the convergence rates of the relative error in energy norm for the uniform and adaptive refinement by the three methods, and the results are shown in Fig. 14. From Fig. 14(c), we observe both the uniform and adaptive collocation methods can yield the optimal convergence rate, and adaptive collocation shows better accuracy due to the efficient refinement strategy. At the last refinement step, adaptive Greville abscissae collocation with 35,388 DOFs results in an error of $1.49 \cdot 10^{-4}$, while the Galerkin method with 34,908 DOFs results in an error of $8.33 \cdot 10^{-6}$ and Gaussian collocation with 35,020 DOFs has an error of $9.04 \cdot 10^{-6}$. A similar pattern but with significantly higher error per degree of freedom can be noticed for uniform refinement.

4.3. L-shaped wedge

Next we consider a benchmark problem of the L-shaped wedge, which contains a singularity at a re-entrant corner in the domain. A plane strain state is assumed. The analytical solution of the problem is given in [49]. The boundary conditions are shown in Fig. 15, and the inner and outer corners are fixed. The L-shaped wedge is discretized into two PHT patches, where each one is a trapezoid. There is a singularity at the inner re-entrant corner. In order to reduce the error from the singularity, we apply the Galerkin method in the 1/4 region for both patches as shown in Fig. 16(a–c). We have removed all the collocation points on the elements where we are using the Galerkin method. To obtain a fully determined linear system, we also remove some of the collocation points on the collocation elements which are next to the Galerkin elements. As can be seen in Fig. 16(d–f), the relative error for the von Mises stress surrounding the singularity is reduced. Fig. 17 shows the convergence rates for both the uniform and adaptive refinement approaches. It is obvious that adaptive refinement improves the accuracy significantly for the three approaches.

4.4. Hollow sphere under internal pressure

Next we solve two 3D examples. First we solve a hollow problem, where the model and the domain geometry are shown in Fig. 18 and Fig. 19 respectively. Note that owing to the symmetrical structure, we consider only one eighth of the original problem. The exact solution [50] is given in terms of spherical coordinates $\{r, \phi, \theta\}$ by

$$u_r = \frac{PR_i^3 r}{E(R_a^3 - R_i^3)} \left((1 - 2\nu) + \frac{(1 + \nu)R_a^3}{2r^3} \right),\tag{27}$$

$$\sigma_r = \frac{PR_i^3 (R_a^3 - r^3)}{r^3 (R_a^3 - R_i^3)},\tag{28}$$

$$\sigma_{\phi} = \sigma_{\theta} = \frac{PR_i^3 (R_a^3 + 2r^3)}{2r^3 (R_a^3 - R_i^3)},$$
(29)

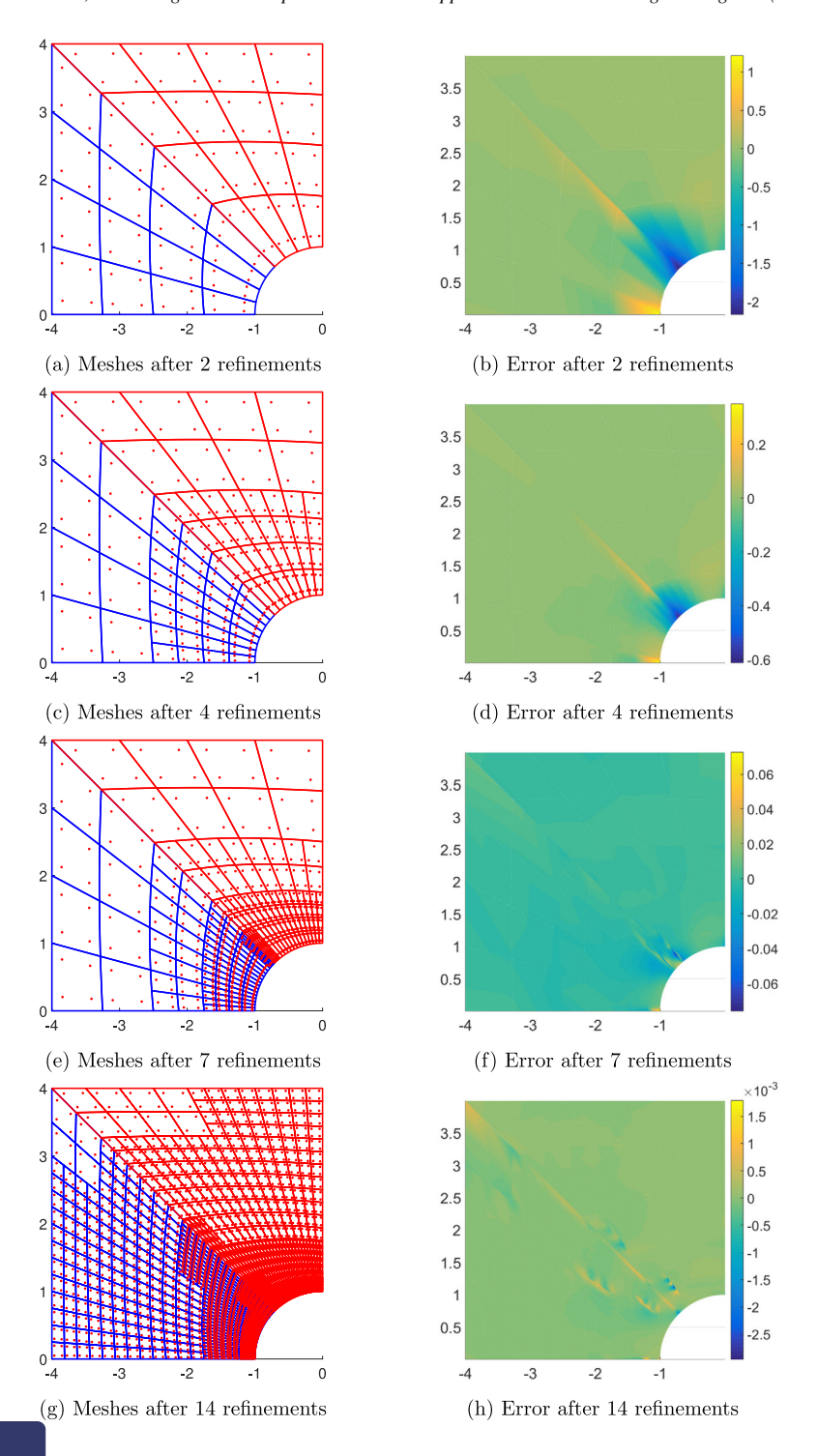
where r and θ are the radius and angle with respect to the origin which is located in the center of the hole. ϕ represents the azimuthal angular in the x-y plane from the x-axis. We let R_a and R_i designate the outer radius and the inner radius, which are given by $R_a = 4$ and $R_i = 1$, respectively. We choose Young's modulus E = 1000, Poisson's ratio v = 0.3

pdfelement

The Trial Version

ed adaptive collocation method to solve the hollow problem, comparing with the uniform error in the energy norm using adaptive and uniform refinements are shown in Fig. 21, and are optimal for the Gaussian collocation and the IGA Galerkin methods. However, Greville a sub-optimal approximation. In addition, Fig. 20 shows results of the refined meshes, the

corresponding von Mises stress and the errors in the stress. As can be observed, the adaptive refinement improves the solution in the region close to the inclusion with significantly fewer degrees-of-freedom compared to uniform



pdfelement
The Trial Version

3. The refined meshes and the error for the stress σ_{xx} in the plate with circular hole example.

Temment. However, there are some localized error hot spots along the patch boundaries and the corner regions. This is because the boundary approximation is somewhat less accurate than the interior region, even with the hybrid

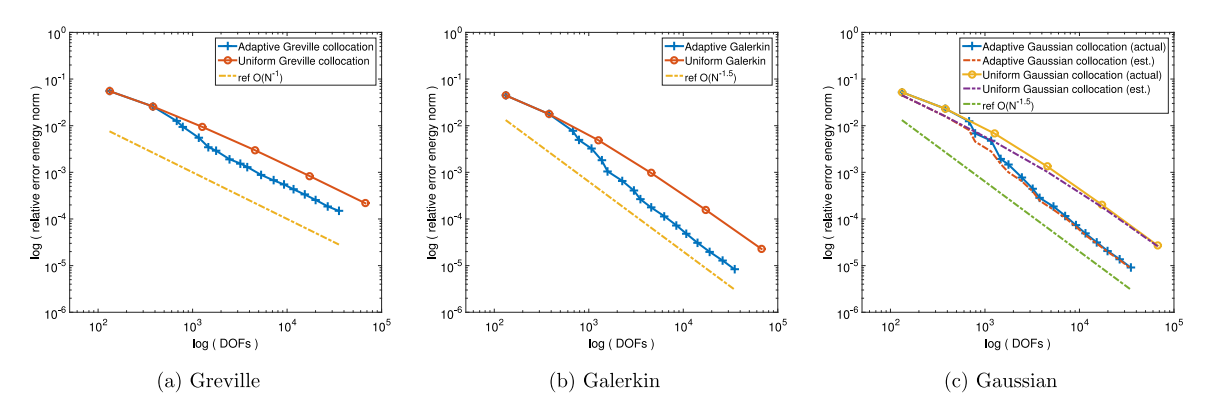


Fig. 14. Relative error (exact and estimated) in energy norm, using adaptive and uniform refinements for the plate with hole example.

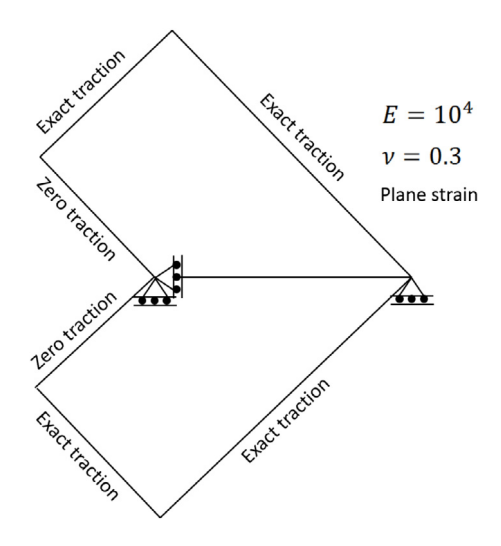


Fig. 15. Problem description for the L-shaped wedge example.

Galerkin technique. Accurate treatment of the Neumann boundary conditions is a challenging research topic for the IGA collocation.

4.5. Spherical hole in an infinite solid subject to uniform tension

Here we consider a cube with an internal spherical hole in an infinite domain in \mathbb{R}^3 , as shown in Fig. 22. The exact stresses, given using the spherical coordinate $\{r, \phi, \theta\}$ by [51,52] are

$$\sigma_{rr} = S\cos^2\theta + \frac{S}{7 - 5\nu} \left(\frac{a^3}{r^3} \left(6 - 5(5 - \nu)\cos^2\theta \right) + \frac{6a^5}{r^5} \left(3\cos^2\theta - 1 \right) \right),\tag{30}$$

$$\begin{array}{ll}
\text{pdfelement} & S \\
\frac{a^3}{r^3} \left(5\nu - 2 + 5(1 - 2\nu)\cos^2\theta\right) + \frac{a^5}{r^5} \left(1 - 5\cos^2\theta\right), \\
\frac{S}{2(7 - 5\nu)} \left(\frac{a^3}{r^3} \left(4 - 5\nu + 5(1 - 2\nu)\cos^2\theta\right) + \frac{3a^5}{r^5} \left(3 - 7\cos^2\theta\right)\right), \\
\end{array} (31)$$

The Trial Version
$$\frac{S}{2(7-5\nu)} \left(\frac{a^3}{r^3} \left(4 - 5\nu + 5(1-2\nu)\cos^2\theta \right) + \frac{3a^5}{r^5} \left(3 - 7\cos^2\theta \right) \right),$$
 (32)

$$\sigma_{r\theta} = S\left(-1 + \frac{1}{7 - 5\nu} \left(-\frac{5a^3(1 + \nu)}{r^3} + \frac{12a^5}{r^5}\right)\right) \sin\theta \cos\theta,\tag{33}$$

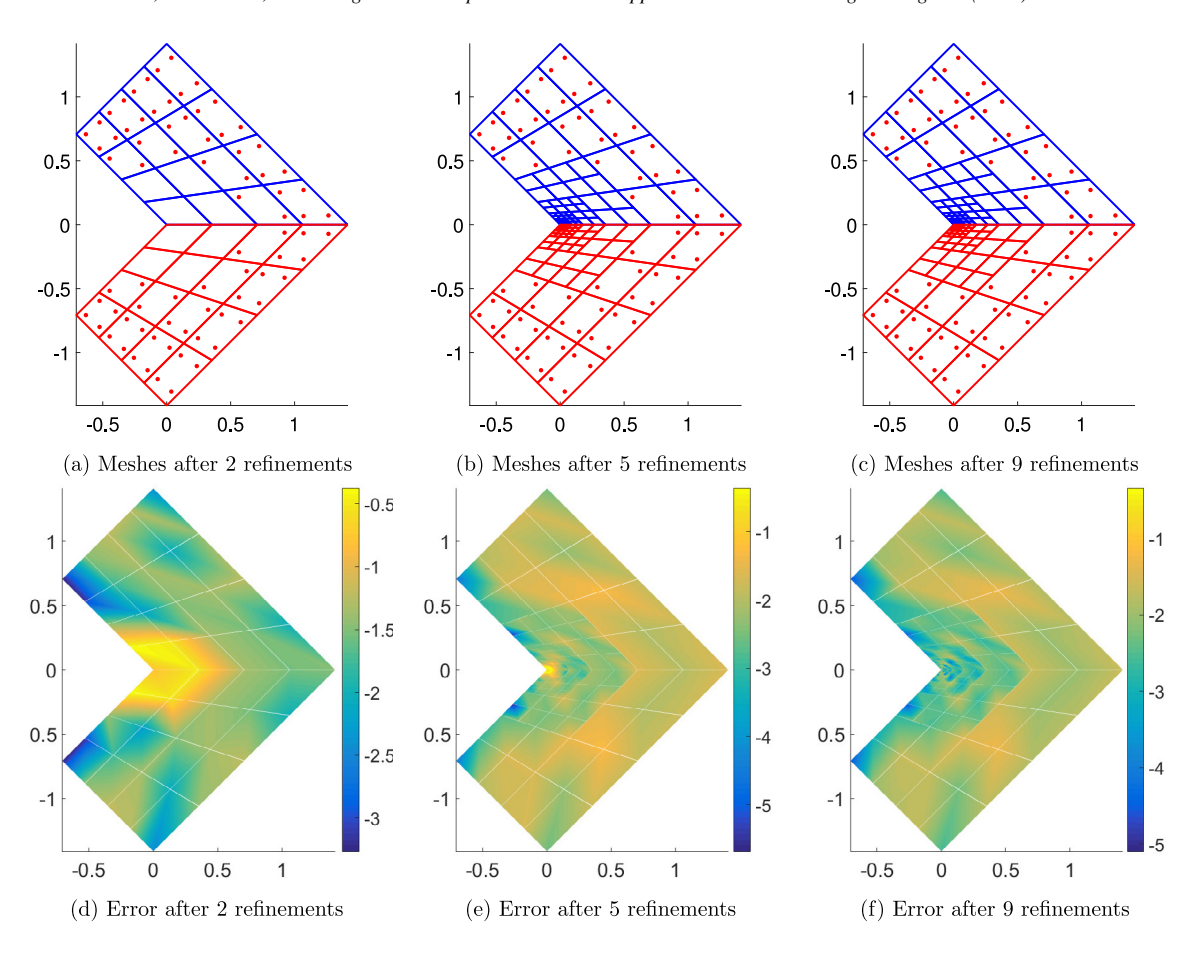
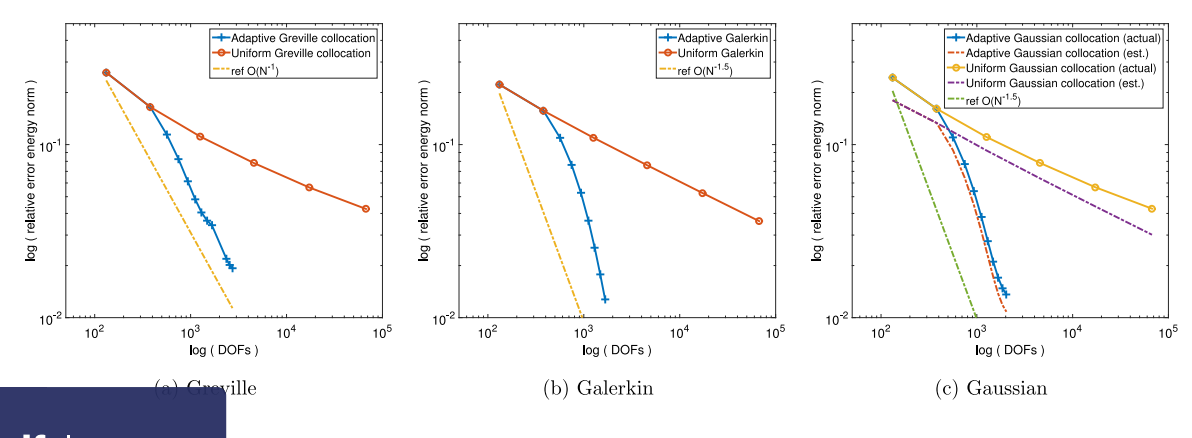


Fig. 16. Relative error for the von Mises stress after several refinement steps. The relative error is plotted in the log scale (base 10).



exact and estimated) in energy norm, using adaptive and uniform refinements for the L-shaped wedge example.

pdfelement

The Trial Version

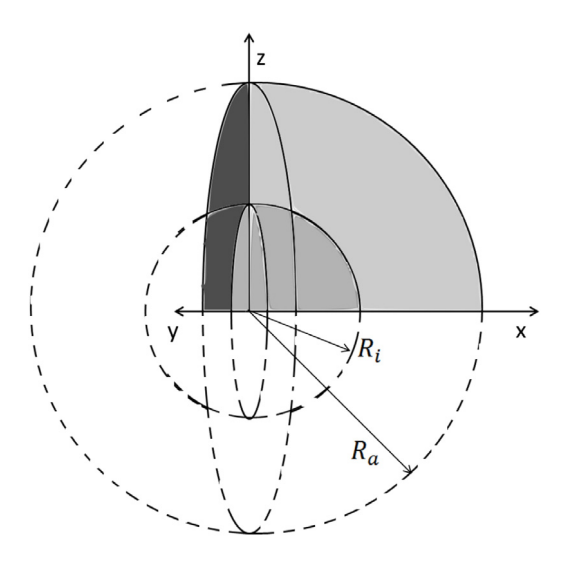


Fig. 18. Problem description for the hemisphere example.

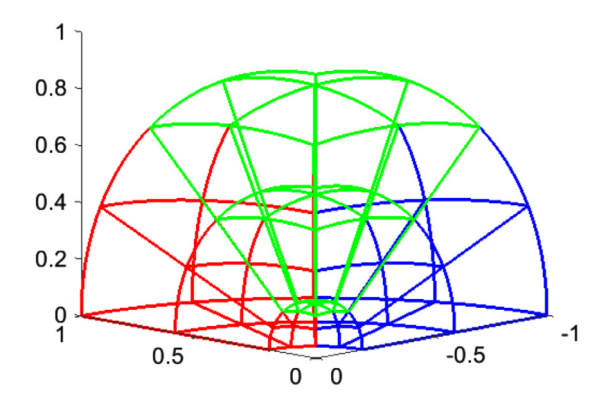


Fig. 19. Three geometric patches for the hollow sphere example.

where a denotes the radius of the sphere. S is the uniaxial tension applied at infinity and μ and ν are the shear modulus and Poisson's ratio respectively.

Because of the symmetry, 1/8 of the problem domain is considered and discretized into three geometric patches as shown in Fig. 23. The stress field in the z-direction and the corresponding errors obtained for fine meshes are plotted in Fig. 24. The convergence plot is shown in Fig. 25. We observe that the optimal convergence rate in terms of degree-of-freedom is obtained for both the uniform and adaptive refinements for the Gaussian collocation and IGA Galerkin approaches, whereas the results of the Greville abscissae are sub-optimal.

5. Conclusion

We have proposed an adaptive IGA collocation method with a recovery-based error estimator. We have chosen cation sites, which are suitable for C^1 bases such as the PHT-splines. However, when adaptive presence of T-junctions results in more Gauss points than basis functions. Thus, we remove the elements surrounding T-junctions in order to have a fully determined matrix system. The Trial Version are positions of the collocation points to ensure they are located at the proper distance from ex. Furthermore, we deal with the boundary conditions in a simple and stable way, by using a

hybrid Galerkin approach for the Neumann and inter-patch boundaries. Finally, we obtain optimal convergence rates (same as with the Galerkin method) for both the uniform and adaptive refinement procedures when solving several

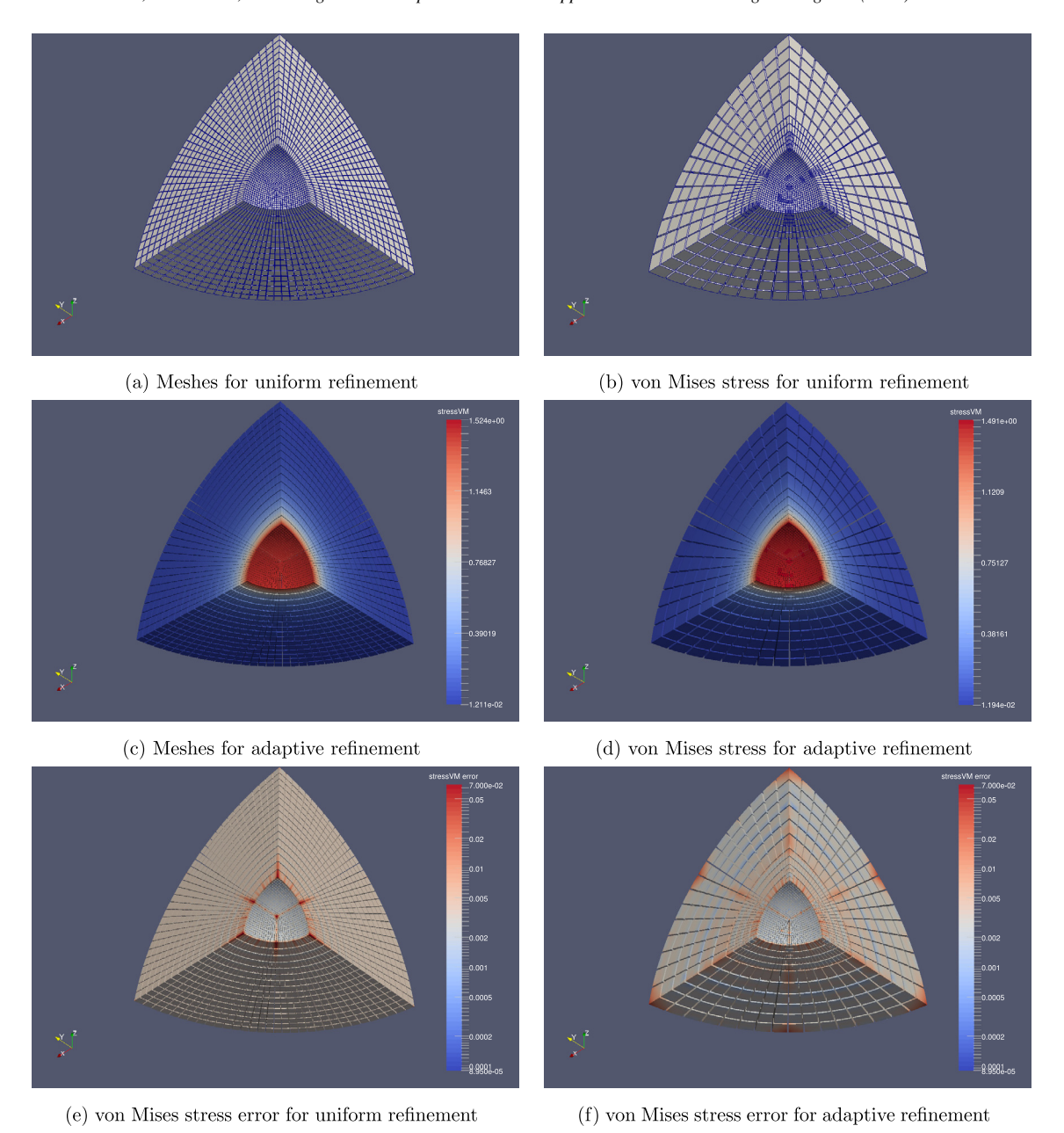


Fig. 20. The von Mises stresses and the refined meshes corresponding to uniform refinement and adaptive refinement for the hemisphere example obtained from the Gaussian collocation method. The number of the DOFs for uniform refinement is 343,434, and the number of the DOFs for adaptive refinement is 143,706.

enchmark problems, including multi-patch domains and re-entrant corners. We also compare n with the traditional Greville collocation and the IGA Galerkin methods.

The Trial Version work, we plan to extend our algorithm to more general higher polynomial degree splines.

Meanwhile, we are planning to enrich our method by combining other techniques, such as XFEM, to model material failure or material interface problems. More complex geometry models and more practical contact problems could be considered in further research work as well.

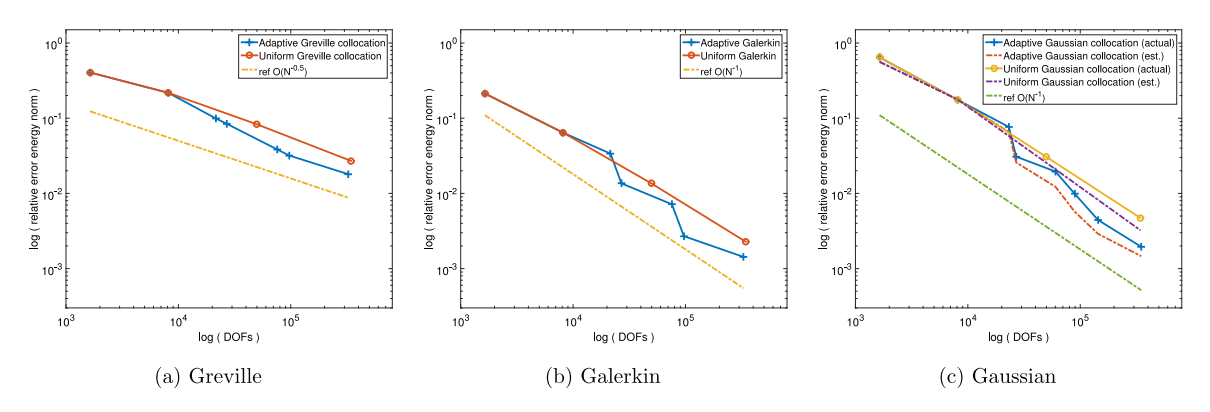


Fig. 21. Relative error (exact and estimated) in energy norm, using adaptive and uniform refinements for the hemisphere example.

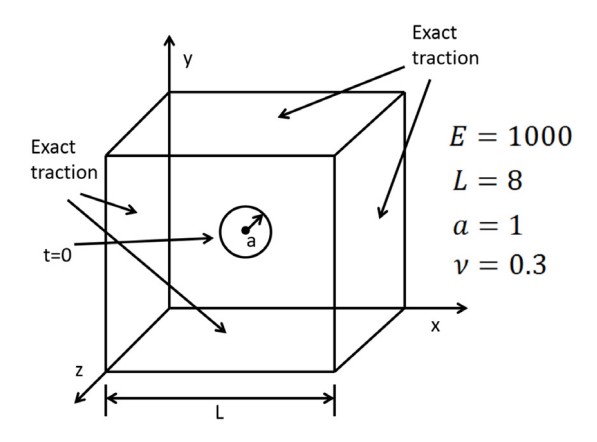


Fig. 22. Problem description for 1/8 of the cube with a spherical hole.

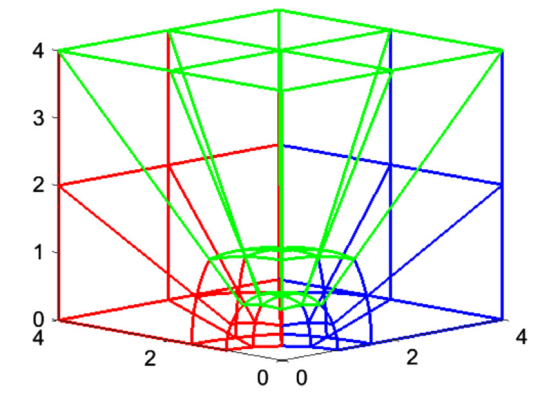




Fig. 23. Three geometric patches for the cube with a spherical hole example.

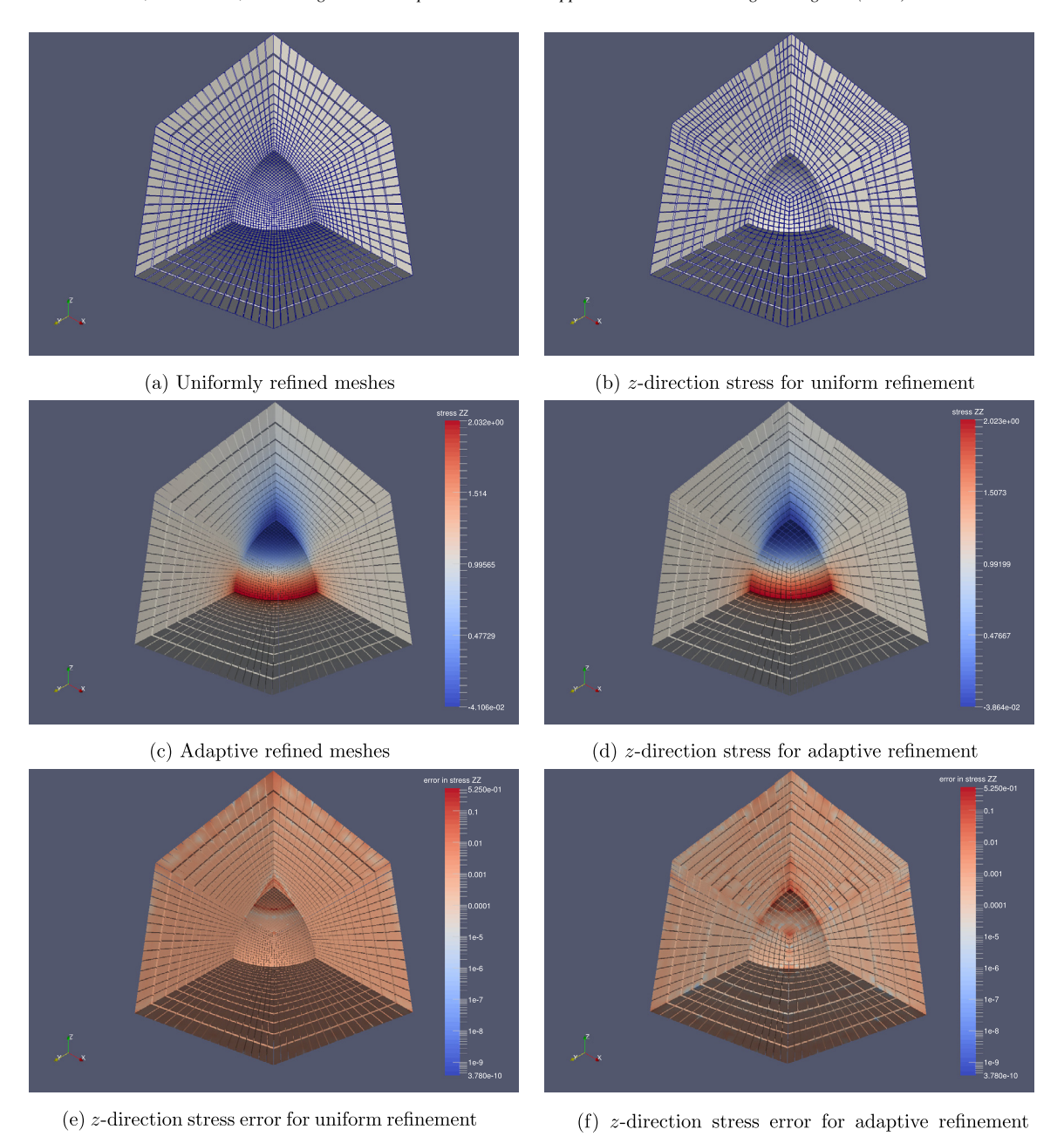


Fig. 24. The stresses in the *z*-direction and the refined meshes corresponding to the uniform and adaptive refinements for the cube with a spherical hole example obtained from the Gaussian collocation method. The number of the DOFs for uniform refinement is 343,434, and the number of the DOFs for adaptive refinement is 212,394.

pdfelement

The Trial Version and Supported by the China Scholarship Council (CSC), the top International University Visiting Research Funds for the Central Universities, China (Nos. 3102017jc01003, 3102017jc11001). Y. Zhang was supported in part by the PECASE award N00014-16-1-2254 (USA), NSF CAREER Award OCI-1149591 (USA) and NSF,

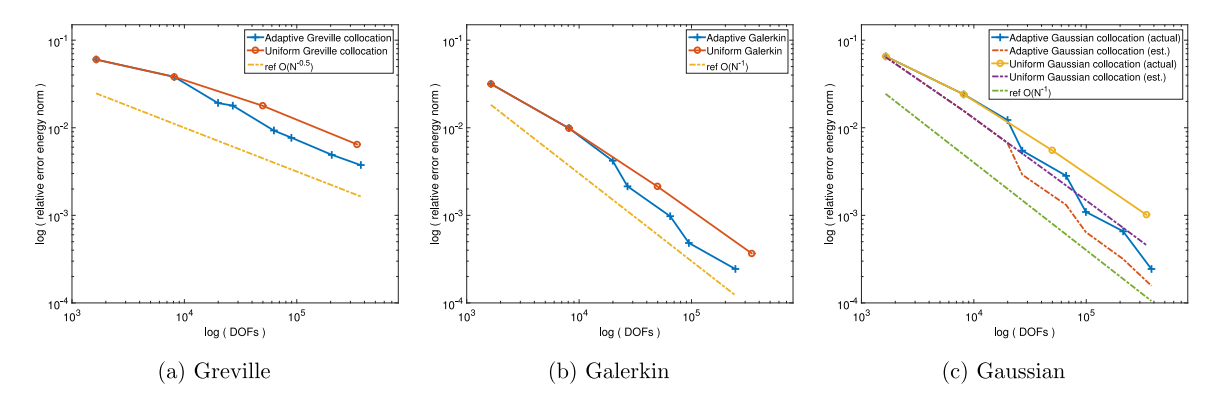


Fig. 25. Relative error (exact and estimated) in energy norm, using adaptive and uniform refinements for the cube with a spherical hole example.

USA grant CBET-1804929. C. Anitescu and T. Rabczuk acknowledge the partial support of the European Union (European Research Council project number 615132) and of the German Research Foundation (DFG project number 392023639).

References

pdfelement

- [1] T.J.R. Hughes, J.A. Cottrell, Y. Bazilevs, Isogeometric analysis: CAD, finite elements, NURBS, exact geometry and mesh refinement, Comput. Methods Appl. Mech. Engrg. 194 (2005) 4135–4195.
- [2] J.A. Cottrell, T.J.R. Hughes, Y. Bazilevs, Isogeometric Analysis, John Wiley & Sons, Ltd, 2009.
- [3] J. Kiendl, M.C. Hsu, M.C. Wu, A. Reali, Isogeometric Kirchhoff-Love shell formulations for general hyperelastic materials, Comput. Methods Appl. Mech. Engrg. 291 (2015) 280–303.
- [4] D.J. Benson, Y. Bazilevs, M.C. Hsu, T.J.R. Hughes, A large deformation, rotation-free, isogeometric shell, Comput. Methods Appl. Mech. Engrg. 200 (13–16) (2011) 1367–1378.
- [5] Y. Lai, Y. Zhang, L. Liu, X. Wei, E. Fang, J. Lua, Integrating CAD with Abaqus: A practical isogeometric analysis software plateform for industrial application, Comput. Math. Appl. 74 (7) (2017) 1648–1660.
- [6] R.L. Taylor, FEAP Finite Element Analysis Program, University of California, Berkeley.2014 http://www.ce.berkeley.edu/feap.
- [7] D.J. Benson, Y. Bazilevs, E. De Luycker, M.C. Hsu, M.A. Scott, T.J.R. Hughes, T. Belytschko, A generalized finite element formulation for arbitrary basis functions: From isogeometric analysis to XFEM, Internat, J. Numer. Methods Engrg. 83 (2010) 765–785.
- [8] T.W. Sederberg, J. Zheng, A. Bakenov, T-splines and T-NURCCs, ACM Trans. Graph. 22 (3) (2003) 477-484.
- [9] X. Li, M.A. Scott, Analysis-suitable T-splines: Characterization, refineability, and approximation, Math. Models Methods Appl. Sci. 24 (6) (2014) 1141–1164.
- [10] E.J. Evans, M.A. Scott, X. Li, D.C. Thomas, Hierarchical T-splines: Analysis suitability, Bézier extraction, and application as an adaptive basis for isogeometric analysis, Comput. Methods Appl. Mech. Engrg. 284 (2015) 1–20.
- [11] J. Deng, F. Chen, X. Li, C. Hu, W. Tong, Z. Yang, Y. Feng, Polynomial splines over hierarchical T-meshes, Graph. Models 70 (4) (2008) 76–86.
- [12] C. Giannelli, B. Jüttler, H. Speleers, THB-splines: The truncated basis for hierarchical splines, Comput. Aided Geom. Design 29 (7) (2012) 485–498.
- [13] T. Dokken, T. Lyche, K.F. Pettersen, Polynomial splines over locally refined Box-partition, Comput. Aided Geom. Design 30 (3) (2013) 331–356.
- [14] X. Wei, Y. Zhang, L. Liu, T.J.R. Hughes, Truncated T-splines: Fundamentals and methods, Comput. Methods Appl. Mech. Engrg. 316 (2017) 349–372.
- [15] L.H. Nguyen, D. Schillinger, A collocated isogeometric finite element method based on Gauss-Lobatto Lagrange extraction of splines, Comput. Methods Appl. Mech. Engrg. 316 (2017) 720–740.
- [16] D. Schillinger, S.J. Hossain, T.J.R. Hughes, Reduced Bézier element quadrature rules for quadratic and cubic splines in isogeometric analysis, Comput. Methods Appl. Mech. Engrg. 277 (2014) 1–45.
 - Element Method: Linear Static and Dynamic Finite Element Analysis, Dover Publicatins, Inc., Mineola, New York,

Efficient quadrature for NURBS-based isogeometric analysis, Comput. Methods Appl. Mech. Engrg. 199 (5-8)

The Trial Version T.J.R. Hughes, A. Reali, G. Sangalli, Efficient quadrature for NURBS-based isogeometric analysis, Comput. Methods -252 (2012) 15–27.

[20] F. Auricchio, L. Beirão da Veiga, T.J.R. Hughes, A. Reali, G. Sangalli, Isogeometric collocation methods, Math. Models Methods Appl. Sci. 20 (11) (2010) 2075–2107.

- [21] F. Auricchio, L. Beirão da Veiga, T.J.R. Hughes, A. Reali, G. Sangalli, Isogeometric collocation for elastostatics and explicit dynamics, Comput. Methods Appl. Mech. Engrg. 249–252 (2012) 2–14.
- [22] L. Beirão da Veiga, C. Lovadina, A. Reali, Avoiding shear locking for the Timonshenko beam problem via isogeometric collocation methods, Comput. Methods Appl. Mech. Engrg. 241–244 (2012) 38–51.
- [23] D. Schillinger, J.A. Evans, A. Reali, M.A. Scott, T.J.R. Hughes, Isogeometric collocation: Cost comparison with Galerkin methods and extension to adaptive hierarchical NURBS discretizations, Comput. Methods Appl. Mech. Engrg. 267 (2013) 170–232.
- [24] H. Li, Q. Hu, Y. Xiong, Consistency and convergence properties of the isogeometric collocation method, Comput. Methods Appl. Mech. Engrg. 267 (2013) 471–486.
- [25] G. Farin, Curves and Surfaces for CAGD, Morgan Kaufmann Publisher, San Francisco, 1999.
- [26] C. Anitescu, Y. Jia, Y. Zhang, T. Rabczuk, An isogeometric collocation method using superconvergent points, Comput. Methods Appl. Mech. Engrg. 284 (2015) 1073–1097.
- [27] H. Gomez, L. De Lorenzis, The variational collocation method, Comput. Methods Appl. Mech. Engrg. 309 (2016) 152–181.
- [28] M. Montardini, G. Sangalli, L. Tamellini, Optimal-order isogeometric collocation at Galerkin superconvergent points, Comput. Methods Appl. Mech. Engrg. 316 (2017) 741–757.
- [29] L. De Lorenzis, J.A. Evans, T.J.R. Hughes, A. Reali, Isogeometric collocation: Neumann boundary conditions and contact, Comput. Methods Appl. Mech. Engrg. 284 (2015) 21–54.
- [30] D. Schillinger, M.J. Borden, H.K. Stolarski, Isogeometric collocation for phase-field fracture models, Comput. Methods Appl. Mech. Engrg. 284 (2015) 583–610.
- [31] I. Babŭska, W.C. Rheinboldt, A-posteriori error estimates for the finite element method, Internat. J. Numer. Methods Engrg. 12 (10) (1978) 1597–1615.
- [32] I. Babŭska, W.C. Rheinboldt, Error estimates for adaptive finite element computations, SIAM J. Numer. Anal. 15 (4) (1978) 736–754.
- [33] C. Anitescu, M.N. Hossain, T. Rabczuk, Recovery-based error estimation and adaptivity using high-order splines over hierarchical T-meshes, Comput. Methods Appl. Mech. Engrg. 328 (2018) 638–662.
- [34] O.C. Zienkiewicz, J.Z. Zhu, The superconvergence patch recovery and a posteriori error estimation in the finite element method, Part 1: The recovery technique, Internat. J. Numer. Methods Engrg. 33 (7) (1992) 1331–1364.
- [35] O.C. Zienkiewicz, J.Z. Zhu, The superconvergence patch recovery and a posteriori error estimation in the finite element method, Part 2: Error estimates and adaptivity, Internat. J. Numer. Methods Engrg. 33 (7) (1992) 1365–1382.
- [36] A. Buffa, D. Cho, M. Kumar, Characterization of T-splines with reduced continuity order on T-meshes, Comput. Methods Appl. Mech. Engrg. 201–204 (2012) 112–126.
- [37] P. Wang, J. Xu, J. Deng, F. Chen, Adaptive isogeometric analysis using rational PHT-splines, Comput. Aided Des. 43 (11) (2011) 1438–1448.
- [38] C. de Boor, B. Schwartz, Collocation at Gaussian points, SIAM J. Numer. Anal. 10 (4) (1973) 582-606.
- [39] H. Casquero, L. Liu, Y. Zhang, A. Reali, H. Gomez, Isogeometric collocation using analysis-suitable T-splines of arbitrary degree, Comput. Methods Appl. Mech. Engrg. 301 (2016) 164–186.
- [40] M.J. Borden, M.A. Scott, J.A. Evans, T.J.R Hughes, Isogeometric finite element data structures based on Bézier extraction of NURBS, Internat. J. Numer. Methods Engrg. 87 (2011) 15–47.
- [41] J.Z. Zhu, O.C. Zienkiewicz, Superconvergence recovery technique and a posteriori error estimators, Internat. J. Numer. Methods Engrg. 30 (7) (1990) 1321–1339.
- [42] I. Babuška, T. Strouboulis, C.S. Upadhyay, S.K. Gangaraj, Computer-based proof of the existence of superconvergence points in the finite element method; superconvergence of the derivatives in finite element solutions of Laplace's, Poisson's, and the elasticity equations, Numer. Methods Partial Differential Equations 12 (3) (1996) 347–392.
- [43] W. Dörfler, A convergent adaptive algorithm for Poisson's equation, SIAM J. Numer. Anal. 33 (3) (1996) 1106-1124.
- [44] S.P. Timoshenko, J.N. Goodier, Theory of Elasticity, third ed., McGraw, 1970.
- [45] I. Babŭska, T. Strouboulis, C.S. Upadhyay, A model study of the quality of a posteriori error estimators for linear elliptic problems. Error estimation in the interior of patchwise uniform grids of triangles, Comput. Methods Appl. Mech. Engrg. 114 (3–4) (1994) 307–378.
- [46] O.A. González-Estrada, J.J. Ródenas, S.P.A. Bordas, M. Duflot, P. Kerfriden, E. Giner, On the role of enrichment and statical admissibility of recovered fields in a-posteriori error estimation for enriched finite element methods, Engineering Computations: International Journal for Computer-Aided Engineering and Software 29 (9) (2012) 814–841.
- [47] H. Kang, J. Xu, F. Chen, J. Deng, A new basis for PHT-splines, Graph. Models 82 (2015) 149–159.
- [48] P.L. Gould, Introduction to Linear Elasticity, Springer-Verlag, 1999.
- [49] B. Szabó, I. Babŭska, Finite Element Analysis, John Wiley and Sons, 1991.
- [50] D. Schillinger, J.A. Evans, F. Frischmann, R.R. Hiemstra, M.C. Hsu, T.J.R. Hughes, A collocated C⁰ finite element method: Reduced quadrature perspective, cost comparison with standard finite elements, and explicit structural dyanmics, Internat. J. Numer. Methods Engrg. 102 (2015) 576–631.
- [51] J.R. Barber, Elasticity, Springer-Verlag New York, 2010.

son, J.A. Evens, S. Lipton, S.P.A. Bordas, T.J.R. Hughes, T.W. Sederberg, Isogeometric boundary element analysis lines, Comput. Methods Appl. Mech. Engrg. 254 (2013) 197–221.

